Yueyang He, Chao Ren, Hugo Wai Leung Mak, Changqing Lin, Zixuan Wang, Jimmy Chi Hung Fung, Yuguo Li, Alexis Kai Hon Lau, Edward Ng. (2021).
Investigations of high-density urban boundary layer under summer prevailing wind conditions with Doppler LiDAR: A case study in Hong Kong.*Urban Climate*. doi: 10.1016/j.uclim.2021.100884

Investigations of high-density urban boundary layer under summer prevailing wind conditions with Doppler LiDAR: A case study in Hong Kong

Yueyang He

Chao Ren

Hugo Wai Leung Mak

Changqing Lin

Zixuan Wang

Jimmy Chi Hung Fung

Yuguo Li

Alexis Kai Hon Lau

Edward Ng

Institute of Environment, Energy and Sustainability, The Chinese University of Hong Kong, New Territories, Hong Kong
Faculty of Architecture, The University of Hong Kong, Pokfulam, Hong Kong Department of Electrical and Electronic Engineering, The University of Hong Kong, Pokfulam, Hong Kong
Department of Geography, The University of Hong Kong, Pokfulam, Hong Kong
Division of Environment & Sustainability, Hong Kong University of Science and Technology, Hong Kong
Department of Mechanical Engineering, The University of Hong Kong, Pokfulam, Hong Kong
Department of Mathematics, Hong Kong University of Science and Technology, Hong Kong
Department of Civil and Environmental Engineering, The Hong Kong University of Science and Technology, Hong Kong
School of Architecture, The Chinese University of Hong Kong, New Territories, Hong Kong j
Institute of Future Cities, The Chinese University of Hong Kong, New Territories, Hong Kong

Corresponding author: Chao Ren, Faculty of Architecture, The University of Hong Kong, Pokfulam, Hong Kong
Email address: renchao@hku.hk (C. Ren).

Submitted to *Urban Climate* November 4 2020
Accepted June 2021

Author Biographies

Yueyang He, PhD, is Research Assistant Professor in the Institute of Environment, Energy and Sustainability and School of Architecture at The Chinese University of Hong Kong, New Territories, Hong Kong. His research interests are in sustainable urban design, planning, and microclimate modeling. His current research topics include high-density urban morphology, pedestrian-level wind environments, upper-air wind profiling using Doppler LiDAR, urban extreme hot weather, and indoor air quality and thermal comfort.

Chao Ren, PhD, is Professor in the Faculty of Architecture at The University of Hong Kong, Pokfulam, Hong Kong. Her research interests are in applied climatology, urban microclimate, and sustainable urban design. Her current research topics include urban heat island mitigation strategies, spatial modeling of heat-health risks in high-density cities, climate-responsive guidelines for subtropical built environments, and ventilation assessment in high-density urban areas.

Hugo Wai Leung Mak, PhD, is Assistant Professor in the Department of Electrical and Electronic Engineering at The University of Hong Kong, Pokfulam, Hong Kong. His research interests are in geoinformatics, data analytics, and environmental informatics. His current research topics include spatial and socio-classification of traffic pollutant emissions and mortality rates in high-density cities, land-use/land-cover change dynamics using remote sensing, and applications of variational autoencoders in urban environmental modeling.

Changqing Lin, PhD, is Assistant Professor in the Division of Environment and Sustainability at The Hong Kong University of Science and Technology, Hong Kong. His research interests are in atmospheric remote sensing and air quality modeling. His current research topics include high-resolution satellite retrievals of PM2.5 concentrations, regional aerosol trends in the Pearl River Delta, health impacts of urban air pollution exposure, and fine-scale exposure assessments in megacities.

Zixuan Wang, PhD, is a researcher in the Department of Geography at The University of Hong Kong, Pokfulam, Hong Kong. Her research interests are in urban climatology and environmental geography. Her current research topics include the urban moisture island phenomenon and its mechanisms in high-rise high-density cities, diurnal humidity profiles under urbanization effects, and interactions between building morphology and local atmospheric conditions.

Jimmy Chi Hung Fung, PhD, is Chair Professor in the Department of Mathematics and Division of Environment and Sustainability at The Hong Kong University of Science and Technology, Hong Kong. His research interests are in atmospheric

modeling, air quality simulation, and climate dynamics. His current research topics include numerical simulations of regional air pollution dispersion, coupled chemical transport models for ozone forecasting, impacts of urbanization on boundary layer meteorology, and ultra-fine resolution modeling for street-level exposure in the Greater Bay Area.

Yuguo Li, PhD, is Chair Professor of Building Environment, Honorary Professor of School of Public Health, Associate Dean (Research) of Engineering. His research interests are in building environment engineering. His current research topics include city climate/environment, environment studies of infection and indoor environment.

Alexis Kai Hon Lau, PhD, is Chair Professor in the Division of Environment and Sustainability and Department of Civil and Environmental Engineering at The Hong Kong University of Science and Technology, Hong Kong. His research interests are in regional air quality, satellite remote sensing, and environmental health. His current research topics include high-resolution mapping of ground-level PM2.5 using MODIS data, source-receptor relationships in the Pearl River Delta, policy impacts on secondary aerosol formation, and long-term exposure effects on lung function and chronic obstructive pulmonary disease.

Edward Ng, PhD, is Yao Ling Sun Professor of Architecture in the School of Architecture and Institute of Future Cities at The Chinese University of Hong Kong, New Territories, Hong Kong. His research interests are in green building, environmental and sustainable design, and urban climatology for city planning. His current research topics include computational analysis of urban ventilation corridors, green infrastructure for heat stress reduction, evidence-based planning for resilient cities, and adaptable frameworks for subtropical low-income housing under future climate scenarios.

Investigations of high-density urban boundary layer under summer prevailing wind conditions with Doppler LiDAR: A case study in Hong Kong

Abstract

The high-density urban boundary layer (UBL) is one of the most complex atmospheric conditions, while the field data of UBL is limited due to the lack of suitable measurement methods. To better understand the UBL structures in high-density cities, a pioneering investigation is conducted in Hong Kong by Doppler wind LiDAR. Vertical wind speed profiles are measured at three locations: Cape D'Aguilar (upwind), University of Hong Kong (downtown), and Hong Kong University of Science and Technology (downwind). To address the weak wind conditions in summer, the prevailing southwest wind condition is selected as the subject of investigation. Based on the observations, the gradient height over Hong Kong is approximately 1.0–1.2 km. Below this height, the vertical wind speed profiles are significantly modified by surface morphologies. The power-law equation appropriately parametrizes the upwind (α =0.1–0.15) and downwind (α = 0.27) profiles, but it has limitations when parametrizing the downtown profile. Deficiencies of the vertical wind speed profiles predicted by conventional meso-scale simulations and wind-tunnel experiments are revealed. These results provide researchers and engineers benchmarking data to refine their urban climate predictions. They generalize a better understanding of the UBL climates, which can be shared with other high-density cities.

(199 words)

Keywords

Urban boundary layer, Wind speed profile, Gradient height, High-density city, Weak wind condition, Doppler LiDAR

1.Introduction

The urban boundary layer (UBL) is that portion of the atmospheric boundary layer above the urban canopy, where the surfaces are inhomogeneous (Oke, 2002). The structure of the UBL is, therefore, highly complex, due to numerous sources and sinks of momentum and heat (Barlow, 2014; Gryning et al., 2011). Some parameters that describe the wind conditions of the UBL, such as the vertical wind speed profiles and gradient height, are essential inputs in urban climate studies, for example, on the predictions of wind behaviors (Blocken and Persoon, 2009; He et al., 2019; Yuan and Ng, 2012), thermal distribution (Uehara et al., 2000; Wang and Ng, 2018) and pollutant dispersions (Blocken et al., 2008; Hang et al., 2012; Tominaga and Stathopoulos, 2018). It has been reported that small errors of these input parameters

can lead to obvious deviations, fluctuations, and even mistaken modelling outputs (Jiang et al., 2008). Therefore, a better understanding of the UBL structures is useful and practical to improve urban climate predictions.

Investigations on the wind characteristics of the UBL are challenging, mainly due to the practical difficulties in estimating or observing the upper-air wind conditions. Investigations of the UBL rely on either simulations or measurements. The simulations are generally considered to be less accurate than measurements, while the conventional observations, such as those on tall towers, balloons or even helicopters (Roth, 2000), are restricted by their durations, frequencies, heights and/or stability. To overcome these restrictions, ground-based remote sensing instruments, such as Doppler wind Light Detection and Ranging (LiDAR), have been introduced into urban climate studies in recent years (Liu et al., 2019). They have been used to investigate the UBL of different cities in the world. For example, in central London, Drew et al. (2013) and Kent et al. (2018) observed the vertical wind speed profiles over several urban areas. They found that a detailed assessment of the nature of urban surfaces is essential, especially when estimating the wind conditions of the UBL. Later, Halios and Barlow (2018) observed the morning transition of the UBL, and found that the nighttime UBL is more convective when compared with the boundary layer over rural areas. In Tokyo, Kikumoto et al. (2017) and Lim et al. (2017) investigated the vertical wind speed profiles under various weather and climatic conditions. Their results revealed that the parameters of the power-law equation are not constant, but rather time-dependent when estimating the UBL. In Houston, Haman et al. (2012) investigated the seasonal variations of the UBL heights in a near-coastal urban area. Their results indicated seasonal and daily variability of the UBL heights caused by thermal instability. In Beijing, Huang et al. (2017) investigated the diurnal cycle of the UBL heights. They proposed composite methods to estimate the UBL heights in convective and neutral cases. In Seoul metropolitan area, Park and Chae (2018) investigated the vertical structures of the land-sea breezes. They observed a reduction of durations of sea breezes against distances from the shoreline. Recently, in Hong Kong, Yim (2020) and Huang et al. (2020) observed the variability of the UBL, particularly in hot-and-polluted and cloudy cases. Their observations mainly provided insights for the studies of transboundary air pollution. The above literatures revealed that the UBL structures varied with surface morphologies, thermal conditions, as well as local circulations. Thus, investigations on the UBL should be conducted on a case-by-case basis. For cities like Hong Kong, which are under the combined effects of high-density surface morphologies, unstable thermal stratifications, and land-sea breeze circulations, investigations on the wind distribution of the UBL are still limited, especially under weak wind conditions during summer.

<Fig.1>

1.2. The need for studying UBL structures of Hong Kong under weak wind conditions

As one of the representative high-density cities in the world, Hong Kong has complex terrains that consist of high-rise buildings and hilly topographies. Neighboring to the Pearl River Delta Region of mainland China on the north and facing the open sea on other sides, Hong Kong has a subtropical and monsoon climate with seasonal changes of wind directions (HKO, 2020a). Hong Kong's climate is famous for hot-humid summer and mild winter. Based on the statistics released by the HKSAR government (HKPD, 2019a), built-up areas occupy only 25% of the total land in the city, while those undeveloped areas are hilly to mountainous regions that consist of steep slopes. Due to the limited urban land resources and dense population, local buildings are usually tall and compact (Ng et al., 2011; Yuan and Ng, 2012). For example, at the downtown of Hong Kong Island, the buildings can have a ground coverage ratio of over 70%, a mean height of over 60 m, and a permissible domestic plot ratio up till 10 (HKPD, 2016). As a consequence, these high-density urban morphologies significantly modify the approaching wind profiles to the city.

In summer (i.e., from June to August in this study), the city is dominated by the prevailing southwest wind coming from the sea, as shown in Fig. 1. During this period, weaker mean wind speed has been recorded in comparison with the corresponding annual data at the near-ground weather stations of the Hong Kong Observatory (HKO) (HKO, 2020b). The HKO's historical data also reveal a dramatic deceleration of the mean wind speed from an upwind to a downtown location. Such a weak wind condition always challenges outdoor thermal comfort (Ren et al., 2021; Shi et al., 2018; Shi et al., 2019a), pollutant dispersion (Shi et al., 2016; Shi et al., 2019b) and human health (Qian et al., 2010; Wang et al., 2019) of a city.

Careful considerations and adaptations of urban designs in respect of the weak background wind conditions become especially important. To address the relevant urban issues, the government has established an air ventilation assessment (AVA) system (HKPD, 2005) and published its technical circular NO. 1/06 (HPLB and ETWB, 2006) since early 2000. This system aims to assess and minimize the potential impacts of the new development and redevelopment of a site on its ambient wind environment. As required, repre sentative vertical wind speed profiles of the site should be set as the boundary conditions in the assessment tools of either boundary layer wind tunnel (BLWT) experiments or computational fluid dynamics (CFD) simulations. In this sense, the knowledge of the input UBL should remain updated in order to guarantee more accurate AVA output.

1.3. Research objectives

As discussed previously, the wind distribution of the UBL are one of the main determinants of urban climate conditions. However, their characteristics, especially those in high-density cities, have not been fully understood due to the limitations of conventional investigation methods. The Doppler wind LiDAR acts as a supplement to the conventional methods of obtaining vertical wind speed profiles with several

advantages, as reviewed in Section 2. A more complete and accurate investigation of the high-density UBL can help researchers and wind engineers to optimize their urban climate predictions. Furthermore, it can also provide information to planners and architects to adjust their designs for better urban ventilation.

To extend the existing knowledge, this study uses Hong Kong as an example to conduct multi-points wind LiDAR measurements over high-density urban morphologies. To address the weak wind conditions in summer, the prevailing southwest wind condition becomes the focus of this study. Based on the new observations, this study aims to 1) characterize the LiDAR vertical wind speed profiles at the upwind, downtown and downwind locations in a high-density city; and 2) reveal the potential deficiencies of the current site wind availability data in Hong Kong (i.e., a set of vertical wind speed profiles predicted by conventional meso-scale simulations and wind-tunnel experiments in the AVA system). It is expected to generalize a better understanding of the complex UBL climates, characterized by high-density surface morphologies, thermal instability and land-sea breeze circulations, which can be shared with other cities in similar conditions.

<Fig.2>

2. Conventional methods of obtaining vertical wind profiles in Hong Kong

2.1. Upper-air sounding measurements

In Hong Kong, several conventional methods have been adopted to obtain the vertical wind speed profiles. These methods include the HKO's upper-air sounding measurements (HKO, 2019), reduced-scale BLWT experiments (CUHK, 2008, 2010), and meso-scale weather simulation models, which include the Regional Atmospheric Modelling System (RAMS) (HKPD, 2013) and Weather Research and Forecasting (WRF) (ENVF and IENV, 2021) models. Amongst these methods, the upper-air sounding measurements have been conducted by the Automatic Upper-air Sounding System at King's Park meteorological station (AUSS KP) (Fig. 2) since 2004. This system launches a hydrogen-filled balloon with radiosondes, to obtain vertical wind data with a climbing speed of around 6 m/s, and a sampling rate of 2 s. The AUSS KP provides reliable upper-air data, but its frequency of launching a balloon is very low (i.e., twice a day at 8.00 am and 8.00 pm). Besides, due to the fixed launcher equipment, the obtained vertical wind profiles are restricted at only a site. Moreover, as reported in previous studies, the spatial drifts of the climbing balloon may sometimes make considerable errors to the data statistics (McGrath et al., 2006; Seidel et al., 2011). With all these limitations, some recent studies (Li and Chan, 2016; Yang et al., 2019; Yim et al., 2007) only adopted the upper-air sounding data for validation purposes.

2.2. Boundary layer wind tunnel experiments

Beside the sounding measurements, the government published a set of experimental or simulated vertical wind speed profiles, named site wind availability data (HKPD, 2019b). The experimental wind availability data was established for 13 sites in 16 cardinal wind directions, via a low-speed BLWT from 2006 to 2009 (CUHK, 2008, 2010). Throughout the experiments, a 40 m long test section was used to develop a vertical wind speed profile approaching the respective site, in accordance with the description of the power-law equation shown in Eq. (1):

$$U = U_{\text{ref}} \left(\frac{z}{z_{\text{ref}}} \right)^{a} \tag{1}$$

where U denotes the magnitude of the horizontal wind speed at different vertical heights(z); U_{ref} represents the reference wind speed at a reference height (z_{ref}), and α is the power-law exponent related to terrain roughness. To reproduce the input wind characteristics over open water, the experiments set U_{ref} (Fig. 2), and α based on the long-term non-typhoon mean wind speed observed at AWS WGL to be 0.15 (i.e., category II in Table 1). A 1: 2000 reduced-scale topographical model was used to determine the effects of topography and urban morphologies within a distance of up to 10 km from the site toward the approaching wind. Miniature dynamic pressure probes were used to record the output vertical wind speed profiles. Despite the lack of data at the heights beyond 0.5 km in full scale, and the lack of consideration of thermal stratification (Wang and Ng, 2018), such experimental site wind availability data has been used as boundary conditions in researches (Du et al., 2017; Letzel et al., 2012; Ng et al., 2011) and AVA practices.

2.3. Meso-scale simulations

As an alternative to the experimental data, the RAMS model was used to produce a simulated 10-year wind climate distribution, with the horizontal resolution of 0.5 km × 0.5 km covering the whole territory of Hong Kong (HKPD, 2013). The model was run in three nested domains, where the lateral boundary conditions were obtained from National Centers for Environmental Prediction (NCEP), with a horizontal resolution of 0.6 degree in latitude and longitude respectively, and a temporal resolution of 6 hours. The terrain height being specified in the model is based on the actual topography, while the mean building height was neglected. Land-use classification algorithms were then applied to obtain land surface types that represent "surface roughness" in the model. The RAMS site wind availability data has been widely used in researches (An et al., 2020; Ng et al., 2012; Thilakaratne et al., 2016) and AVA practices. However, it is known to have limitations. For example, it only provides the annual full mean wind profiles as well as the summer and winter mean wind statistics at limited vertical levels, while the real-time information is lacked.

Also, there is a lack of wind data at the heights beyond 0.5 km. Beside the RAMS model, the WRF model (ENVF and IENV, 2021) has been increasingly used to predict real- time meteorological conditions in Hong Kong (Wang et al., 2018; Wong et al., 2019). In the WRF model, four nested domains with horizontal grid resolutions of 27 km, 9 km, 3 km, and 1 km were used. The lateral boundary conditions were obtained from NCEP with a horizontal resolution of 1 degree in latitude and longitude, and a temporal resolution of 6 hours. To represent the urban surface roughness, the WRF model is coupled with the multi-layer building effect parameterization and the building energy model urban scheme. As suggested in literature, such urban scheme can provide better simulations of wind speed, and obtain slight improvement in retrieving temperature distribution over urban areas. However, meso-scale simulations may have simplified the physical and morphological features of complex terrain, thus affecting the accuracies of near-ground attributes (Ribeiro et al., 2018; Wong et al., 2019).

<Table.1>

2.4. Pros and cons of different methods

Table 2 summarizes the pros and cons of all aforementioned methods of obtaining vertical wind profiles in Hong Kong, along with the new Doppler LiDAR approach. Compared with the conventional techniques, the Doppler wind LiDAR approach is preferable in conducting long-term investigations of higher stability and reliability. More importantly, the LiDAR instruments have relatively higher movability and lower relocation cost, which makes it possible to collect wind availability data of more sites. Therefore, this new method can act as an important supplement to the conventional methods, so that a better understanding of the wind characteristics of the UBL in Hong Kong can be achieved.

<Table.2>

3. New method of investigating the UBL via the use of LiDAR

3.1. Study sites: locations and surrounding environments

To measure the real-site vertical wind profiles, long-range LiDAR units (Leosphere WindCube 100S) were installed at three lo cations in Hong Kong, namely Cape D'Aguilar (LiDAR CDA), the Yam Pak building rooftop at the University of Hong Kong (LiDAR HKU), and the air quality research supersite at the Hong Kong University of Science and Technology (LiDAR UST). As shown in Fig. 2, the LiDAR at CDA is located at an undeveloped peninsula in southeastern Hong Kong Island, which is surrounded by an open sea in the south and west; the LiDAR at HKU is located at the downtown of northwestern Hong Kong Island, characterized by high-

rise buildings and hilly topographies; and the LiDAR at UST is located at a suburban area in eastern New Territories, facing to the sea bay in the east.

The relative locations of these three LiDAR units are depicted in Fig. 3. When the prevailing southwest wind approaches Hong Kong in summer, LiDAR CDA was at an upwind location of the city. Wind profiles recorded at this location received relatively low interference from topographies due to the upwind open sea. In comparison, LiDAR HKU was tasked to measure wind profiles at the downtown, where wind conditions were assumed to be heavily affected and modified by high-density urban morphologies. Meanwhile, LiDAR UST was located at the downwind side of the city. At this location, the wind had already passed through the urban areas with the highest roughness and was re-adapted to the environmental conditions of the suburban areas.

3.2. Setup of Doppler LiDAR units

In this study, all LiDAR units adopted the Doppler beam swinging (DBS) scan mode to reconstruct the vertical profiles of horizontal wind speed. As shown in Fig. 4, a DBS scan cycle rotates at four azimuths, namely east, south, west, and north, in approximately 20s. At each azimuth, the laser pulse is emitted to the upper-air from the oscillator. Part of the laser pulse is then backscattered by the aerosols and captured by the receiver. The wind-induced particle movements result in Doppler shift (Δf), which is calculated by Eq. 2:

$$\Delta f = f - f_0 \tag{2}$$

where f and f_0 are the received and emitted frequencies of the laser pulse, respectively. The radial wind speed at each height up to 3 km above ground was calculated proportionally to the detected Δf, and then converted into the horizontal wind speed components at corresponding height, by Eqs. (3) – (5):

$$u = 0.5(V_{RE} - V_{RW}) / \sin\gamma \tag{3}$$
$$v = 0.5(V_{RN} - V_{RS}) / \sin\gamma \tag{4}$$

<Fig.3>

<Fig.4>

$$U = \sqrt{u^2 + v^2} \tag{5}$$

where, u and v are the east-west horizontal and north-south horizontal components of the wind speed; V_{RE}, V_{RW}, V_{RN} and V_{RS} are the radial wind speeds along the east-tilted, west-tilted, north-tilted and south-tilted directions; and γ is the half cone angle

(chosen as 15◦ within this study). The wavelength of the emitted laser pulse was set to be 1.54μm so that the effective transmission of the optical signals in the upper-air and eye safety of users can be guaranteed (Thobois et al., 2019). The reported measurement accuracy of the radial wind speed is around 0.5 m/s at the range between 0 and 115 m/s (Leosphere, 2020). Meanwhile, the vertical wind shear profiles can be estimated by Eq. (6) (Li et al., 2017):

$$S = \frac{U_{\text{high}} - U_{\text{low}}}{z_{\text{high}} - z_{\text{low}}} \tag{6}$$

where S is the horizontal wind shear at different vertical heights (z); U_{high} and U_{low} are the horizontal wind speeds at the higher and lower levels of z, respectively; and z_{high} and z_{low} are the two levels that the wind speeds are obtained. The strength of the wind shear is affected by the thickness between the two levels (i.e., $z_{\text{high}} - z_{\text{low}}$). Referring to the recommendation by Li et al. (2017), this study sets z_{high} and z_{low} to be 25 m above and below z, respectively. Noted that 25 m is precisely one vertical measurement interval of LiDAR in the current scan mode.

3.3. Study period: selection of sampling data with a prevailing southwest wind

The measurements were conducted from 1 June to 31 August in 2020, which covers the entire summer period of the year. Since this study only focused on the wind that approaches Hong Kong in the southwest direction, the period with approaching wind from other directions were excluded from the study period. In this study, the southwest approaching wind is defined as the wind from directions between the south (180◦) and west (270◦) based on the data recorded at AWS WGL. It should be noted that when the southwest wind is approaching Hong Kong, the wind direction measured by the LiDAR units may not be southwest due to the modifying effects caused by surrounding terrains. Besides, to eliminate the disturbance of abnormal wind condition, three periods of Typhoon NURI (i.e., from 8 pm, 12 June to 1 pm, 14 June), SINLAKU (i.e., 8 pm, 31 July to 11 pm, 1 August), and HIGOS (i.e., from 4 am, 18 August to 1 pm, 19 August) (HKO, 2020c) were also excluded from the study period. Table 3 summarizes the statistics of different wind conditions on an hourly basis during the entire measurement period.

<Table.3>

4. Validation of wind profiles derived from LiDAR measurements

4.1. Data quality control of LiDAR units

The three LiDAR units have been calibrated by the manufacturer with a certified LiDAR unit (R^2 =0.99) before their on-site installations. Since LiDAR adopts remote sensing principles to detect optical signals back-scattered by aerosols, its accuracy of data measurements may be reduced under adverse weather conditions such as rainy and cloudy conditions (Liu et al., 2019). To control and ensure data quality of LiDAR outputs, a minimum threshold value of the carrier-to-noise ratio (CNR) is required to discard data with relatively low accuracies. The effects of CNR on LiDAR data quality have been discussed in previous researches (Beck and Kühn, 2017; Goit et al., 2020). They found that a higher threshold CNR value can indeed increase the accuracy of measurements, but at the same time sacrificing the number of available data points. To balance the data quality and data availability under local weather conditions, the minimum threshold CNR value was set as 27 dB within the current study. Similar threshold values were adopted in some latest researches (Beck and Kühn, 2017; Kikumoto et al., 2017).

The HKO's statistics (HKO, 2020b) of the daily average cloud coverage and total rainfall during the entire study period are presented in Fig. 5. Overall, the frequency of the rainy condition is low, indicating that raindrops may have limited interference on data detection of LiDAR measurements. However, almost half of the sampling days have high cloud coverage (i.e., quantified by over 80% as adopted by Yim (2020)). It is known that the laser pulse is not able to penetrate through thick clouds, because of its strong attenuation (WMO, 2014), thus the quality and availability of some LiDAR data at the upper-air could be affected. As explained by HKO (2020d), the annual average cloud coverage has a generally increasing trend in Hong Kong, probably due to the rapid urbanization and human activities that took place within the region. As a result, LiDAR data detections were affected most at the downtown location. However, due to the lack of observation data of the cloud base height at the selected downtown location, the impacts of clouds cannot be quantified in this study, and remains to be a potential future study direction for in-depth analyses.

4.2. LiDAR near-ground upwind data versus Waglan Island wind measurements

To further ensure the accuracy of LiDAR data, on-site validations were conducted by comparing the LiDAR data with other wind measurements in Hong Kong at both near-ground and upper height levels. Firstly, the wind data measured by LiDAR CDA at the height of 50 m was compared with the measurements at AWS WGL (56 m above sea level). Based on available data of the two sources in June, the normalized root mean square error (NRMSE) of the horizontal hourly mean wind speed and direction are 13.1% and 8.3%, respectively. Fig. 6 compares the two sources of hourly mean wind speed and direction during the last week of June 2020. The results indicate a fair agreement between LiDAR data and the data obtained from the local automatic weather station. Slightly larger deviations are observed in wind direction than wind speed, possibly because of the effects of the mountainous terrain that surrounds

LiDAR CDA. However, in overall, the wind data measured by LiDAR CDA serve as good estimates of the natural wind profiles approaching Hong Kong.

4.3. LiDAR downtown wind profiles versus HKO upper-air sounding wind profiles

In the vertical dimension, LiDAR data was compared with the sounding wind data at AUSS KP, which is the only alternative source of upper-air wind measurement in Hong Kong, as described in Section 2.1. The LiDAR data measured at the downtown location was intentionally selected to minimize the effects of different categories of surrounding terrains on data comparisons. At AUSS KP, the radiosondes were actually launched at 7.20 am/pm, and reaches the height of 1.5 km at around 7.24 am/pm for the sounding data at 8 am/pm. To accurately align with the sounding data, the mean and standard deviation of the LiDAR data between 7.20 am/pm and 7.25 am/pm are used in the comparisons. Based on the statistics obtained in June, the NRMSE of horizontal mean wind speed and direction at vertical heights below 0.5 km are 31.1% and 14.5%, respectively. However, their NRMSE decreases to 18.2% and 7.2%, respectively, at vertical elevations from 0.5 km to 1.5 km. Fig. 7 compares the vertical wind profiles between the two data sources in the last week of June, while the corresponding profiles of wind direction are shown in Fig. 8. Due to the effects of different surrounding terrains, the agreement between these two sources of vertical wind profile at lower heights is low. However, the wind profiles measured by LiDAR are still considered trustworthy because of the higher degree of agreements obtained at upper heights, especially for the comparisons of wind direction, as shown in Fig. 8. The larger deviations of wind speed may partly be attributed to the possible horizontal displacements of the climbing balloon (McGrath et al. , 2006; Seidel et al., 2011), as discussed in Section 2.1.

<Fig.5>

<Fig.6>

5. Results and analysis

5.1. Distribution of natural wind availability at different sites

The distribution of hourly mean wind speed recorded by AWS WGL at the height of 0.05 km and the three LiDAR units at the height of 0.5 km are shown in Fig. 9. During the study period, the wind speed of all sites experiences a downward trend from June to August. At the site of near-ground height (AWS WGL), over 80% of the approaching wind speed ranges from 2 m/s to 8 m/s, with the highest frequency at 6 m/s. There are only around 4% of wind speed exceeding 10 m/s. At the other three LiDAR locations, the wind speed is more frequently distributed, with around 65% of wind speed ranging from 5 m/s to 9 m/s, while more than 15% of wind speed data is higher than 10 m/s. Despite the effect of vertical heights, all measurement locations

show a consistent and roughly equivalent distribution in wind speed, except the differences in wind speed at individual sites.

5.2. Mean wind speed profiles at upwind, downtown, and downwind locations

The vertical hourly mean wind speed and shear profiles measured by the three LiDAR at upwind, downtown, and downwind lo cations during the study period are presented in Fig. 10. It is clearly visible that the surrounding terrain has modified the shapes of the vertical wind speed profiles, where the mean wind speeds decrease gradually from the upper to near-ground heights. Amongst the three profiles, the downtown wind speed profile, which was measured over the roughest elements of high-rise buildings and hilly topographies, experiences the lowest near-ground wind speed (1.7 m/s). In contrast, the upwind wind speed profile remains the highest wind speed (6.2 m/s) at the near-ground height due to the relatively flat terrain nearby. The mean wind speeds of the three profiles at upper heights become similar and have relatively small variations against altitudes. Based on the observation of the wind shear profiles, the gradient height is approximately 1.0 km to 1.2 km where the shear stress approaches zero. In addition, it should be noted that relatively huge variations of upper wind speed and wind shear were observed at the downtown location, possibly due to the relatively higher uncertainties of measurements, as discussed in Section 4.1.

To parametrize the spatial effects of the terrain on vertical wind profiles, this study adopted various exponents of terrain roughness listed in Table 1, together with the use of Eq. 1 to estimate the power-law wind profiles. Fig. 11 shows the corresponding wind profiles at different values of α. The mean wind speed at 1 km above ground was treated as the reference wind speed in the estimation. At the upwind location, the power-law wind profile with α estimation with α =0.15 well fits the LiDAR wind profile at most of the vertical heights, while the =0.10 better fits the measured wind speed near the ground. This observation is consistent with the descriptions of the natural wind speed profile approaching Hong Kong in previous wind tunnel benchmarking studies (CUHK, 2008, 2010). It is also in line with the open terrains described in categories I and II in Table 1 (AIJ, 2015), where there are no significant or with few obstructions nearby.

In comparison, at the downtown location, the power-law wind profile with α =0.35, which is recommended for the city center in category V, overestimates the mean wind speed near the ground. Still, it underestimates the mean wind speed at the upper heights. With α =0.50, the power-law wind profile better matches the measured mean wind speed near the ground. However, it leads to a larger underestimation of mean wind speed at upper vertical heights. At the downwind location, the LiDAR wind profile is best fitted by the power-law wind profile with α =0.27, representing the city terrain in category IV of Table 1.

5.3. Diurnal variations of mean wind speed

The hourly mean wind speed profiles measured by the three LiDAR are categorized into daytime and nighttime in Fig. 12. Based on the sunrise and sunset time of summer in Hong Kong, “daytime” is defined as the period from 6 am to 7 pm, while the remaining time period is defined as “nighttime”. At the upwind location, where ambient wind receives relatively less influence by urban terrains, the mean wind speed at daytime is larger than its counterpart at all vertical heights. Near the ground level, the difference in mean wind speed between daytime and nighttime is less than 0.5 m/s, while such difference can increase up to more than 1.5 m/s. A similar phenomenon can be observed during the previous summer in Hong Kong (Huang et al., 2020; Yim, 2020). The difference of the vertical wind speed profiles during the daytime and nighttime has been addressed in previous studies (Halios and Barlow, 2018; Haman et al., 2012; Huang et al., 2017). According to these studies, the main reason that leads to the diurnal variations of wind speed is the transformation between convective and neutral conditions. Beside this reason, the current study also intends to address another possible reason that the approaching wind to Hong Kong might be enhanced by the sea-land breeze occurring in the daytime. Due to the significant temperature difference between the sea and the land at hot summer days, the sea breeze is driven toward Hong Kong Island, which is situated in the south of Hong Kong (Liu and Chan, 2002; Lu et al., 2009). This sea-land breeze seems to be integrated with the prevailing southwest wind, as a result enhancing the natural approaching wind during the daytime.

<Fig.8>

Although the daytime approaching wind is enhanced, it hardly makes any changes to the near-ground mean wind speed, because of the influences of surrounding urban terrains. At the downtown and downwind locations, the mean wind speed during the daytime is only slightly larger than its nighttime counterpart near the ground. Beyond the vertical heights of 0.3 km, the wind is even weaker during the daytime compared to nighttime. This can be explained by the radiation of heat energy that takes place in infrastructures and other urban surfaces during nighttime (Wong and Steve, 2010). The release of heat energy interferes with the initial temperature inversion at the near-ground atmosphere (Li et al., 2007), and eventually enhances airflow movements. As a result, it causes mixing between different vertical layers during nighttime. In this study, stronger interference can be observed in the downtown area than the downwind suburban area.

Fig. 13 shows the diurnal variations of mean wind speed at various vertical levels. The mean wind speed at the upwind location experiences huge fluctuations at all vertical heights, and these fluctuations generally follow a similar trend. It reaches a peak in the early afternoon when solar radiation is the strongest, and it gradually decreases until reaching a trough at midnight. In comparison, the changes in wind speed at downtown and downwind locations are relatively flat, especially at the lower

vertical levels, suggesting that the wind in the downtown is somehow decoupled from the upstream winds. Besides, a slight peak of mean wind speed can be observed after sunrise at locations situated next to the sea, i.e., at both upwind and downwind locations, which may be caused by the influences of land-sea breeze during nighttime. After sunrise, the temperature difference between the sea and the land starts to decrease with increasing solar radiation, thus resulting in a decrease in wind speed when compared to the peak value.

5.4. Comparisons of wind profiles from LiDAR, BLWT, RAMS, and WRF methods

One of the purposes of this study is to reveal the potential limitations or deficiencies of the experimental (i.e., BLWT) and simulated wind profiles (i.e., RAMS and WRF), which are frequently used in outdoor ventilation and pollution dispersion studies, as well as in AVA practices. It is assumed that the wind profiles measured by LiDAR are more reliable and consist of relatively fewer assumptions when compared to wind profiles obtained by experimental methods or from simulations. Thus, LiDAR mean wind speed profiles are used as the baseline to evaluate the accuracy of wind profiles estimated by other methods, as shown in Fig. 14. To obtain a fair comparison, all wind speed profiles were normalized by their wind speed at the height of 0.5 km. Besides, the estimated experimental or simulated wind speed profiles were obtained from the site that is nearest to the LiDAR locations. To be more specific, the BLWT wind profiles (wind direction: averaged from 180 ° to 270 °) of Sheung Wan and Tseung Kwan O (CUHK, 2008, 2010) were scaled to represent the wind conditions at the downtown, and downwind locations, respectively; the RAMS wind profiles referred to the simulated annual full mean wind profiles (wind direction: sector from 202.5 ° to 292.4°) at the model girds that the corresponding LiDAR unit is located. WRF wind profiles were derived from the real-time (i.e., from June to August 2020) meteorological simulations (wind direction: averaged from 180° to 270°) at the model girds that the corresponding LiDAR unit is located.

<Fig.9>

<Fig.10>

<Fig.11>

<Fig.12>

As noticed from Fig. 14, a common problem of the experimental and simulated wind profiles is that they underestimate the wind availability at heights above 0.5 km. At these heights, the deviation of wind velocity ratio can be over 25%. At the lower vertical heights, the performance of simulated and experimental wind profiles varies at different locations. At the upwind location, the WRF wind profiles are almost consistent with the LiDAR wind profiles, while the RAMS wind profiles show a clear

underestimation. At the downtown and downwind locations, the RAMS wind profiles have the best agreements with the LiDAR wind profiles. However, in contrast, the wind tunnel and WRF wind profiles tend to have underestimations and overestimations, respectively. In particular, a considerable deviation can be detected at the downwind location based on WRF outputs, possibly due to the lack of representation of the unresolved topography in WRF modelling processes.

<Fig.13>

<Fig.14>

6. Discussion

6.1. Holistic understandings of urban wind conditions in summer

This study addresses the weak wind conditions under the southwest prevailing wind direction in Hong Kong during the summer of 2020. Under the tropical climatic conditions, the local wind is considered to be "the more, the better" within this season (Ng, 2009). It has been widely accepted that urban wind conditions are associated with human comfort and health (Goggins et al., 2012). Within this study, results show that when the southwest approaching wind decelerated from June to July and August, as shown in Fig. 9, the number of very hot days became tripled (HKO, 2020e), and the number of hot nights significantly increased (HKO, 2020f). As a result, an increase in illness and deaths have become severe consequences in our society (Ren et al., 2021; Wang et al., 2019).

The results of this study allow to conclude that the natural wind availability from the southwest direction is adequate to ventilate the sites during most dates in the summer before it is altered by the presence of urban terrains (He et al., 2018; Yuan and Ng, 2012). With reference to the recordings at AWS WGL, a place that has uninterrupted exposure to the wind experiences a prevailing wind speed in the range of 2 m/s to 8 m/s at the near-ground level (Fig. 10). Such wind speed range is higher than the minimum wind speed threshold for achieving thermal comfort during human outdoor activities, which is above 1.3 m/s to 1.5 m/s (Cheng et al., 2012; HKPD, 2008). Therefore, the results, to some extents, imply the possibilities for urban planners and architects to improve the local wind and thermal environment, by taking good use of the natural wind sources in Hong Kong, even during summer.

6.2. Parametrization of wind speed profiles and UBL heights over high-density urban morphologies

Much of the earlier urban wind studies conducted in Hong Kong and other high-density cities of the world were developed by assuming specific characteristics of local UBL. Due to the complex urban morphology and high-density built environment

of Hong Kong, it is always difficult for researchers to obtain the exact vertical distribution of wind speeds and determine the real UBL heights at target sites. Thus, researchers have to rely on the semi-empirical power-law or log-law equations to estimate the vertical wind profiles, as proposed by available standards and guidelines (AIJ, 2015; Franke and Baklanov, 2007; SA and SNZ, 2002; Tominaga et al., 2008). The only drawback of using these equations is that the real-world situations may have been simplified during the process.

With the use of available LiDAR measurements, this study has established a better and clear understanding of how high-density urban morphologies alter wind distribution at different vertical heights. This can be valuable to future climatology studies and investigations in Hong Kong and other high-density cities. The use of LiDAR measurement datasets provides an important baseline for parametrizing the structures of the UBL. In the case of Hong Kong in this study, the presence of built-up areas seriously affects the approaching wind profiles, with the maximum mean wind speed reduced by over 4 m/s, as illustrated in Fig. 10. These modified wind profiles in different terrains can be roughly described by the revised power-law equation, with values of α listed in Table 4. The values determined in this study generally agree with the suggested values stated in AIJ (2015). However, such a method should be carefully considered for applications in downtown areas, because it will lead to apparent underestimation of vertical wind speed, as shown in Fig. 11. A better alternative method to reconstruct the downtown wind profiles in urban climate modelling systems is to directly interpolate the wind profiles measured by LiDAR, through appropriate numerical schemes.

Based on the observation of the wind shear profiles estimated by available LiDAR measurement data (Fig. 10), the gradient height is around 1 km to 1.2 km when surface stress is absent. Above this height, the mean wind speed possesses only relatively slight fluctuations with vertical heights. This value of the gradient height is similar to the one (around 1 km) obtained by another recent study in Hong Kong (Huang et al., 2020). It is also within the reasonable ranges of UBL height measured by LiDAR instruments in other cities, such as Beijing (0.3 km to 1.5 km) (Huang et al., 2017) and London (0.3 km to 1.2 km) (Kent et al., 2018). Besides, the estimated UBL height within this study is found to be larger than the commonly-used empirical value for city centers (0.65 km), as recommended by AIJ (2015). This implies that the popular empirical value may have underestimated the amount of surface stress over Hong Kong's high-density urban morphologies, though such value has been widely adopted in CFD simulations. However, to more precisely identify the exact UBL height in Hong Kong, further validations have to be conducted, especially taking into account both turbulence and temperature gradient thresholds (Dai et al., 2014).

<Table.4>

6.3. Limitations of existing site wind availability data in local urban climate researches and AVA practices

In this study, higher spatial and temporal resolution LiDAR measurements act as supplements of experimental and simulated wind profiles in Hong Kong. By treating LiDAR data as the baseline, this study further reveals and identifies the limitations of the existing data sources that are frequently used in outdoor wind and air pollutant dispersion studies, as well as in AVA. The main deficiency of experimental and simulated data sources is that they fail to consider or underestimate the wind speeds at vertical levels that exceed 0.5 km, as illustrated in Fig. 14. These upper-air wind conditions may potentially affect the transboundary behaviors of airflow and air pollutants in a larger spatial scale (Welford et al., 2006), and therefore further investigations become necessary. At vertical heights below 0.5 km, compared with the experimental wind profiles, the simulated wind profiles are more consistent with the LiDAR observations. However, based on previous experience, the wind tunnel benchmarking data should be considered as a more reliable source compared with the simulated data. One reason of the larger deviations of the experimental data is that the number of available sites in wind tunnel experiments (i.e., 13 sites) is far less than those obtained from RAMS (i.e., 0.5 km × 0.5 km in whole territory) and WRF methods (i.e., 1 km × 1 km in whole territory). As a result, when compared to the situations of simulated wind profiles, the location of selected sites for obtaining experimental wind profiles are further from the actual locations of the imposed LiDAR units. To better understand the rationale behind, further studies should be conducted to the potential impacts on the urban ventilation by adopting wind profiles derived from different approaches.

6.4. Generalization of the wind characteristics of high-density UBL climates during summer

With a case-based observation in Hong Kong, this study generalizes the wind characteristics of UBL over high-density cities. These characteristics are the complex integration of the influence of high-density built environment, thermal instability and local circula tions. High-density built environment is the principal determinant of such wind characteristics, since it affects the stratification of airflow and heat (Gronemeier et al., 2017; Gryning et al., 2011) and further enhances the local atmospheric instability in both temporal and spatial dimensions. Additionally, the interactions between urban terrains and land-sea cycles can be considerable (Lu et al., 2009; Ribeiro et al., 2018). In the case of Hong Kong, the weaker influence of land-sea breeze circulations seems to be observed over high- density built environment compared with relatively open terrain as indicated in Fig. 13. The general understanding of high-density UBL climates observed in this study is helpful to the local urban climate predictions, and furthermore, it can be shared with other cities in similar conditions. However, the current study is only focusing on the prevailing southwest wind in summer. Therefore, further investigations should be conducted in

other seasons under different prevailing wind conditions to have a more comprehensive understanding of high-density UBL climates.

7. Conclusion and future extensions

With Doppler wind LiDAR, this study conducts field measurements of vertical mean wind speed profiles at three different locations in Hong Kong, namely Cape D'Aguilar (upwind), the University of Hong Kong (downtown), and the Hong Kong University of Science and Technology (downwind), during the summer in 2020. The purpose of this study is to better understand the wind characteristics of the high-density UBL under the summer prevailing wind, and meanwhile to provide more precise wind profiles for researches and practices in Hong Kong. To ensure the measurement accuracy, LiDAR data is validated by HKO upper-air sounding data and near-ground data at Waglan Island. Results show that the presence of built-up areas significantly modifies the mean wind speed profiles approaching Hong Kong. At the near-ground height, the difference in mean wind speed between the upwind and downtown locations can be up to 4 m/s, and such difference decreases with increasing heights up to approximately 1.2 km of the gradient height. The power-law estimation is found to appropriately quantify the wind profiles at the upwind ($\alpha = 0.1–0.15$) and downwind ($\alpha = 0.27$) locations. However, it fails to fit the wind profile at the downtown location. Besides, diurnal variations of wind profiles are also observed, with the maximum fluctuation occurring at the upwind location. Using LiDAR data as the baseline, this study further identifies the limitations of existing experimental and simulated wind profiles for conducting urban ventilation and pollutant dispersion studies, as well as for AVA practice in Hong Kong. With the supplements of LiDAR measurements, climatology researchers and wind engineering scientists can better understand local wind distribution, and refine their urban climate modelling accordingly. Thereafter, planners and architects will potentially obtain more precise site wind availability data, which are useful for making wise and appropriate decisions that help to improve urban air ventilation in the long run. Furthermore, the case-based observations in this study generalize a better understanding of the wind characteristics of UBL climates over high-density cities that can be shared with other cities in similar conditions. This understanding becomes the starting point to investigate the complex interactions amongst high- density built environment, thermal instability and land-sea breeze circulations. Eventually, the knowledge will serve the general aim of developing a more livable built environment in high-density cities.

Authorship statement

Conception and design of study: Yueyang He, Chao Ren, Hugo Wai Leung Mak, Changqing Lin, Zixuan Wang, Edward Ng; acquisition of data: Changqing Lin, Hugo Wai Leung Mak, Zixuan Wang, Jimmy Chi Hung Fung; analysis and/or interpretation of data: Yueyang He, Chao Ren, Hugo Wai Leung Mak, Edward Ng;.

Drafting the manuscript: Yueyang He, Chao Ren, Hugo Wai Leung Mak, Changqing Lin, Zixuan Wang, Jimmy Chi Hung Fung, Yuguo Li, Alexis Kai Hon Lau, Edward Ng; revising the manuscript critically for important intellectual content: Yueyang He, Chao Ren, Hugo Wai Leung Mak, Edward Ng.

Approval of the version of the manuscript to be published (the names of all authors must be listed): Yueyang He, Chao Ren, Hugo Wai Leung Mak, Changqing Lin, Zixuan Wang, Jimmy Chi Hung Fung, Yuguo Li, Alexis Kai Hon Lau, Edward Ng.

Declaration of Competing Interest

The authors declare that they have no known competing financial interests or personal relationships that could have appeared to influence the work reported in this paper.

Acknowledgement
The study is supported by the CUHK Research Sustainability of Major RGC Funding Scheme (CRF-2016/17-C4020-16G-3133195). It is also partially supported by the RIF project named 'Increasing the Resilience to the Health Impacts of Extreme Weather on Elderly People under Future Climate Change (CUHK R4046-18)'.

References

AIJ, 2015. AIJ Recommendations for Loads on Buildings. Architectural Institute of Japan (AIJ), Japan.

An, K., Wong, S.-M., Fung, J.C.H., Ng, E., 2020. Revisit of prevailing practice guidelines and investigation of topographical treatment techniques in CFD-based air ventilation assessments. Build. Environ. 169, 106580.

Barlow, J.F., 2014. Progress in observing and modelling the urban boundary layer. Urban Clim. 10, 216–240.

Beck, H., Kühn, M., 2017. Dynamic data filtering of long-range Doppler LiDAR wind speed measurements. Remote Sens. 9 (6), 561.

Blocken, B., Persoon, J., 2009. Pedestrian wind comfort around a large football stadium in an urban environment: CFD simulation, validation and application of the new Dutch wind nuisance standard. J. Wind Eng. Ind. Aerodyn. 97 (5–6), 255–270.
Blocken, B., Stathopoulos, T., Saathoff, P., Wang, X., 2008. Numerical evaluation of pollutant dispersion in the built environment: comparisons between models and experiments. J. Wind Eng. Ind. Aerodyn. 96 (10 11), 1817–1831.

Cheng, V., Ng, E., Chan, C., Givoni, B., 2012. Outdoor thermal comfort study in a sub-tropical climate: a longitudinal study based in Hong Kong. Int. J. Biometeorol. 56 (1), 43–56.

CUHK, 2008. Working paper 2B: Wind Tunnel Benchmarking Studies – Batch I, Urban Climatic Map and Standards for Wind Environment – Feasibility Study. The Chinese University of Hong Kong (CUHK), Hong Kong. Retrieved from.

CUHK, 2010. Working Paper 2C: Wind Tunnel Benchmarking Studies – Batch II, Urban Climatic Map and Standards for Wind Environment – Feasibility Study. The Chinese University of Hong Kong (CUHK). Retrieved from.

Dai, C., Wang, Q., Kalogiros, J., Lenschow, D., Gao, Z., Zhou, M., 2014. Determining boundary-layer height from aircraft measurements. Bound.-Layer Meteorol. 152 (3), 277–302.

Drew, D.R., Barlow, J.F., Lane, S.E., 2013. Observations of wind speed profiles over greater London, UK, using a Doppler lidar. J. Wind Eng. Ind. Aerodyn. 121, 98–105.
Du, Y., Mak, C.M., Kwok, K., Tse, K.-T., Lee, T.-c., Ai, Z., Liu, J., & Niu, J., 2017. New criteria for assessing low wind environment at pedestrian level in Hong Kong. Build. Environ. 123, 23–36.

ENVF, IENV, 2021. HKUST Real Time MM5/WRF Simulations. Hong Kong: Environmental Central Facility (ENVF) and Institute for the Environment (IENV). Retrieved October 15, 2020, from. http://envf.ust.hk/.

Franke, J., Baklanov, A., 2007. Best Practice Guideline for the CFD Simulation of Flows in the Urban Environment: COST Action 732 Quality Assurance and Improvement of Microscale Meteorological Models. Meteorological Institute, University of Hamburg, Germany.

Goggins, W.B., Chan, E.Y., Ng, E., Ren, C., Chen, L., 2012. Effect modification of the association between short-term meteorological factors and mortality by urban heat islands in Hong Kong. PLoS One 7 (6), e38551.

Goit, J.P., Yamaguchi, A., Ishihara, T., 2020. Measurement and prediction of wind fields at an offshore site by scanning Doppler LiDAR and WRF. Atmosphere 11 (5), 442.

Gronemeier, T., Raasch, S., Ng, E., 2017. Effects of unstable stratification on ventilation in Hong Kong. Atmosphere 8 (9), 168.

Gryning, S.-E., Batchvarova, E., Quante, M., Matthias, V., 2011. Evaluation of Vertical Profiles in Mesoscale Meteorological Models Based on Observations for the

COST728 Study of Winter 2003 PM Episodes in Europe Air Pollution Modeling and its Application XXI. Springer, pp. 499–503.

Halios, C.H., Barlow, J.F., 2018. Observations of the morning development of the urban boundary layer over London, UK, taken during the ACTUAL project. Bound.-Layer Meteorol. 166 (3), 395–422.

Haman, C.L., Lefer, B., Morris, G.A., 2012. Seasonal variability in the diurnal evolution of the boundary layer in a near-coastal urban environment. J. Atmos. Ocean. Technol. 29 (5), 697–710.

Hang, J., Li, Y., Sandberg, M., Buccolieri, R., Di Sabatino, S., 2012. The influence of building height variability on pollutant dispersion and pedestrian ventilation in idealized high-rise urban areas. Build. Environ. 56, 346–360.

He, Y., Tablada, A., Wong, N.H., 2018. Effects of non-uniform and orthogonal breezeway networks on pedestrian ventilation in Singapore's high-density urban environments. Urban Clim. 24, 460–484.

He, Y., Tablada, A., Wong, N.H., 2019. A parametric study of angular road patterns on pedestrian ventilation in high-density urban areas. Build. Environ. 151, 251–267.

HKO, 2019. Upper-Air Weather Measurements in Hong Kong. Hong Kong Observatory (HKO), Hong Kong. Retrieved October 15, 2020, from. https://www.hko.gov.hk/en/wservice/tsheet/uamet.htm. HKO, 2020a. Climate of Hong Kong. Hong Kong Observatory (HKO), Hong Kong. Retrieved October 15, 2020, from. https://www.hko.gov.hk/en/cis/climahk.htm.

HKO, 2020b. Climatological database. Hong Kong Observatory (HKO), Hong Kong. Retrieved October 15, 2020, from. https://www.hko.gov.hk/en/cis/climat.htm.
HKO, 2020c. Tropical Cyclone Warning Signals. Hong Kong Observatory (HKO), Hong Kong. Retrieved October 15, 2020, from. https://www.hko.gov.hk/en/wxinfo/climat/warndb/warndb1.shtml?opt=1&sgnl=1.or.higher&start_ym=202006&end_ym=202008&submit=Submit+Query.

HKO, 2020d. Climate Change in Hong Kong: Cloud Amount, Solar Radiation and Evaporation. Hong Kong Observatory (HKO), Hong Kong. Retrieved October 15, 2020, from. https://www.hko.gov.hk/en/climate_change/obs_hk_cloud.htm. HKO, 2020e. Number of Very Hot Days Observed at the Hong Kong Observatory since 1884. Hong Kong Observatory (HKO), Hong Kong. Retrieved October 15, 2020, from. https://www.hko.gov.hk/en/cis/statistic/vhotday_statistic.htm.

HKO, 2020f. Number of Hot Nights Observed at the Hong Kong Observatory since 1884. Hong Kong Observatory (HKO), Hong Kong. Retrieved October 15, 2020, from. https://www.hko.gov.hk/en/cis/statistic/hngtday_statistic.htm.

HKPD, 2005. Final Report: Feasibility Study for Establishment of Air Ventilation Assessment System. Hong Kong Planning Department (HKPD), Hong Kong. Retrieved from. http://www.pland.gov.hk/pland_en/p_study/comp_s/avas/papers&reports/final_report.pdf.

HKPD, 2008. Final Report: Urban Climatic Map and Standards for Wind Environment - Feasibility Study. Hong Kong Planning Department (HKPD), Hong Kong. Retrieved from. http://www.pland.gov.hk/pland_en/p_study/prog_s/ucmapweb/ucmap_project/content/reports/Comfort_Level_Survey.pdf.

HKPD, 2013. Final Report: Site Wind Availability System and Web-Based Site Wind Availability Database, Consultancy Study on Establishment of Simulated Site Wind Availability Data for Air Ventilation Assessments in Hong Kong. Hong Kong Planning Department (HKPD), Hong Kong. Retrieved from. https://www.pland.gov.hk/pland_en/p_study/comp_s/InceptionReport_webpage_11-12/final_report.pdf.

HKPD, 2016. Chapter 2: Residential Densities, Hong Kong Planning Standards and Guidelines. Hong Kong Planning Department (HKPD), Hong Kong. Retrieved from. https://www.pland.gov.hk/pland_en/tech_doc/hkpsg/full/pdf/ch2.pdf.

HKPD, 2019a. Land Utilization in Hong Kong 2018. Hong Kong Planning Department (HKPD), Hong Kong. Retrieved October 15, 2020, from. https://www.pland.gov.hk/pland_en/info_serv/statistic/landu.html.

HKPD, 2019b. Site Wind Availability Data. Hong Kong Planning Department (HKPD), Hong Kong. Retrieved October 15, 2020, from. https://www.pland.gov.hk/pland_en/info_serv/site_wind/index.html.

HPLB, ETWB, 2006. Technical circular no. 1/06: Air Ventilation Assessments. Housing, Planning and Lands Bureau (HPLB) and Environment, Transport and Works Bureau (ETWB), Hong Kong. Retrieved from. https://www.devb.gov.hk/filemanager/en/content_679/hplb-etwb-tc-01-06.pdf.

Huang, M., Gao, Z., Miao, S., Chen, F., LeMone, M.A., Li, J., Hu, F., Wang, L., 2017. Estimate of boundary-layer depth over Beijing, China, using Doppler lidar data during SURF-2015. Bound.-Layer Meteorol. 162 (3), 503–522.

Huang, T., Yim, S.H.-L., Yang, Y., Lee, O.S.-M., Lam, D.H.-Y., Cheng, J.C.-H., Guo, J., 2020. Observation of turbulent mixing characteristics in the typical daytime cloud-topped boundary layer over Hong Kong in 2019. Remote Sens. 12 (9), 1533.
Jiang, X., Wiedinmyer, C., Chen, F., Yang, Z.L., Lo, J.C.F., 2008. Predicted impacts of climate and land use change on surface ozone in the Houston, Texas, area. J. Geophys. Res. Atmos. 113 (D20).

Kent, C.W., Grimmond, C.S.B., Gatey, D., Barlow, J.F., 2018. Assessing methods to extrapolate the vertical wind-speed profile from surface observations in a city Centre during strong winds. J. Wind Eng. Ind. Aerodyn. 173, 100–111.

Kikumoto, H., Ooka, R., Sugawara, H., Lim, J., 2017. Observational study of power-law approximation of wind profiles within an urban boundary layer for various wind conditions. J. Wind Eng. Ind. Aerodyn. 164, 13–21.

Leosphere, 2020. WindCube Scan. Retrieved October 15, 2020, from. https://www.leosphere.com/products/windcube-scan/.

Letzel, M.O., Helmke, C., Ng, E., An, X., Lai, A., Raasch, S., 2012. LES case study on pedestrian level ventilation in two neighbourhoods in Hong Kong. Meteorol. Z. 21 (6), 575–589.

Li, L., Chan, P.W., 2016. LIDAR observation and numerical simulation of vortex/wave shedding at the eastern runway corridor of the Hong Kong international airport. Meteorol. Appl. 23 (3), 379–388.

Li, S., Li, Y., Tsui, K., 2007. Radioactivity in the atmosphere over Hong Kong. J. Environ. Radioact. 94 (2), 98–106.

Li, Z., Lyu, S., Wen, L., Zhao, L., Ao, Y., Wang, S., 2017. Effect of a cold, dry air incursion on atmospheric boundary layer processes over a high-altitude lake in the Tibetan plateau. Atmos. Res. 185, 32–43.

Lim, J., Akashi, Y., Ooka, R., Kikumoto, H., Choi, Y., 2017. A probabilistic approach to the energy-saving potential of natural ventilation: effect of approximation method for approaching wind velocity. Build. Environ. 122, 94–104.

Liu, H., Chan, J.C., 2002. An investigation of air-pollutant patterns under sea–land breezes during a severe air-pollution episode in Hong Kong. Atmos. Environ. 36 (4), 591–601.

Liu, Z., Barlow, J.F., Chan, P.-W., Fung, J.C.H., Li, Y., Ren, C., Mak, H.W.L., Ng, E., 2019. A review of progress and applications of pulsed Doppler wind LiDARs. Remote Sens. 11 (21), 2522.

Lu, X., Chow, K.C., Yao, T., Fung, J.C., Lau, A.K., 2009. Seasonal variation of the land-sea breeze circulation in the pearl river delta region. J. Geophys. Res. Atmos. 114 (D17).

McGrath, R., Semmler, T., Sweeney, C., Wang, S., 2006. Impact of balloon drift errors in radiosonde data on climate statistics. J. Clim. 19 (14), 3430–3442.

Ng, E., 2009. Policies and technical guidelines for urban planning of high-density cities–air ventilation assessment (AVA) of Hong Kong. Build. Environ. 44 (7), 1478–1488.

Ng, E., Yuan, C., Chen, L., Ren, C., Fung, J.C., 2011. Improving the wind environment in high-density cities by understanding urban morphology and surface roughness: a study in Hong Kong. Landsc. Urban Plan. 101 (1), 59–74.

Ng, E., Chen, L., Wang, Y., Yuan, C., 2012. A study on the cooling effects of greening in a high-density city: An experience from Hong Kong. Build. Environ. 47, 256–271.

Oke, T.R., 2002. Boundary Layer Climates. Routledge.
Park, M.-S., Chae, J.-H., 2018. Features of sea–land-breeze circulation over the Seoul metropolitan area. Geosci. Lett. 5 (1), 1–12.

Qian, H., Li, Y., Seto, W., Ching, P., Ching, W., Sun, H., 2010. Natural ventilation for reducing airborne infection in hospitals. Build. Environ. 45 (3), 559–565.
Ren, C., Wang, K., Shi, Y., Kwok, Y.T., Morakinyo, T., Lee, T.-c., & Li, Y., 2021. Investigating the urban heat and cool island effects during extreme heat events in high density cities: A case study of Hong Kong from 2000–2018. Int. J. Climatol. (under review) 1–19. https://doi.org/10.1002/joc.7222.

Ribeiro, F.N., de Oliveira, A.P., Soares, J., de Miranda, R.M., Barlage, M., Chen, F., 2018. Effect of sea breeze propagation on the urban boundary layer of the metropolitan region of Sao Paulo, Brazil. Atmos. Res. 214, 174–188.

Roth, M., 2000. Review of atmospheric turbulence over cities. Q. J. R. Meteorol. Soc. 126 (564), 941–990. SA, SNZ, 2002. Australia/New Zealand Standard, Structural Design Actions Part 2: Wind Actions, AS/NZS 1170.2:2002. Standards Australia/Standards New Zealand (SA/SNZ), Australia and New Zealand.

Seidel, D.J., Sun, B., Pettey, M., Reale, A., 2011. Global radiosonde balloon drift statistics. J. Geophys. Res. Atmos. 116 (D7).
Shi, Y., Lau, K.K.-L., Ng, E., 2016. Developing street-level PM2. 5 and PM10 land use regression models in high-density Hong Kong with urban morphological factors. Environ. Sci. Technol. 50 (15), 8178–8187.

Shi, Y., Katzschner, L., Ng, E., 2018. Modelling the fine-scale spatiotemporal pattern of urban heat island effect using land use regression approach in a megacity. Sci. Total Environ. 618, 891–904.

Shi, Y., Ren, C., Cai, M., Lau, K.K.-L., Lee, T.-C., Wong, W.-K., 2019a. Assessing spatial variability of extreme hot weather conditions in Hong Kong: a land use regression approach. Environ. Res. 171, 403–415.

Shi, Y., Ren, C., Lau, K.K.-L., Ng, E., 2019b. Investigating the influence of urban land use and landscape pattern on PM2. 5 spatial variation using mobile monitoring and WUDAPT. Landsc. Urban Plan. 189, 15–26.

Thilakaratne, R., Chu, P., Xiao, Y., 2016. Optimization of Hong Kong residential building design guidelines to improve urban air ventilation. In: Paper Presented at the 50th International Conference of the Architectural Science Association 2016. The University of Adelaide, Australia.

Thobois, L., Cariou, J.P., Gultepe, I., 2019. Review of lidar-based applications for aviation weather. Pure Appl. Geophys. 176 (5), 1959–1976.

Tominaga, Y., Stathopoulos, T., 2018. CFD simulations of near-field pollutant dispersion with different plume buoyancies. Build. Environ. 131, 128–139.

Tominaga, Y., Mochida, A., Yoshie, R., Kataoka, H., Nozu, T., Yoshikawa, M., Shirasawa, T., 2008. AIJ guidelines for practical applications of CFD to pedestrian wind environment around buildings. J. Wind Eng. Ind. Aerodyn. 96 (10–11), 1749–1761.

Uehara, K., Murakami, S., Oikawa, S., Wakamatsu, S., 2000. Wind tunnel experiments on how thermal stratification affects flow in and above urban street canyons. Atmos. Environ. 34 (10), 1553–1562.

Wang, W., Ng, E., 2018. Air ventilation assessment under unstable atmospheric stratification—a comparative study for Hong Kong. Build. Environ. 130, 1–13.

Wang, R., Ren, C., Xu, Y., Lau, K.K.-L., Shi, Y., 2018. Mapping the local climate zones of urban areas by GIS-based and WUDAPT methods: a case study of Hong Kong. Urban Clim. 24, 567–576.

Wang, D., Lau, K.K.-L., Ren, C., Goggins, W.B.I., Shi, Y., Ho, H.C., Lee, T.-C., Lee, L.-S., Woo, J., Ng, E., 2019. The impact of extremely hot weather events on all-cause mortality in a highly urbanized and densely populated subtropical city: a 10-year time-series study (2006–2015). Sci. Total Environ. 690, 923–931.

Welford, R., Hills, P., Lam, J., 2006. Environmental reform, technology policy and transboundary pollution in Hong Kong. Dev. Chang. 37 (1), 145–178.

WMO, 2014. Guide to Meteorological Instruments and Methods of Observation. World Meteorological Organization (WMO), Geneva, Switzerland.

Wong, N.H., Steve, K.J., 2010. Air temperature distribution and the influence of sky view factor in a green Singapore estate. J. Urban Plan. Dev. 136 (3), 261–272.

Wong, M.M.F., Fung, J.C.H., Ching, J., Yeung, P.P.S., Tse, J.W.P., Ren, C., Wang, R., Cai, M., 2019. Evaluation of uWRF performance and modeling guidance based on WUDAPT and NUDAPT UCP datasets for Hong Kong. Urban Clim. 28, 100460.

Yang, Y., Yim, S.H., Haywood, J., Osborne, M., Chan, J.C., Zeng, Z., Cheng, J.C., 2019. Characteristics of heavy particulate matter pollution events over Hong Kong and their relationships with vertical wind profiles using high-time-resolution Doppler lidar measurements. J. Geophys. Res. Atmos. 124 (16), 9609–9623.

Yim, S.H.L., 2020. Development of a 3D real-time atmospheric monitoring system (3DREAMS) using Doppler LiDARs and applications for long-term analysis and hot-and-polluted episodes. Remote Sens. 12 (6), 1036.

Yim, S.H., Fung, J.C., Lau, A.K., Kot, S.C., 2007. Developing a high-resolution wind map for a complex terrain with a coupled MM5/CALMET system. J. Geophys. Res. Atmos. 112 (D5).

Yuan, C., Ng, E., 2012. Building porosity for better urban ventilation in high-density cities–a computational parametric study. Build. Environ. 50, 176–189.

Fig. 1. Hong Kong's summer wind rose and summer/annual mean wind speed in the past two decades (2000–2019). The upwind and downtown wind data are recorded at Waglan Island (AWS WGL: 56 m above sea level) and King's Park (AWS KP: 65 m above sea level) automatic weather station (Fig. 2), respectively. (For interpretation of the references to colour in this figure legend, the reader is referred to the web version of this article.)

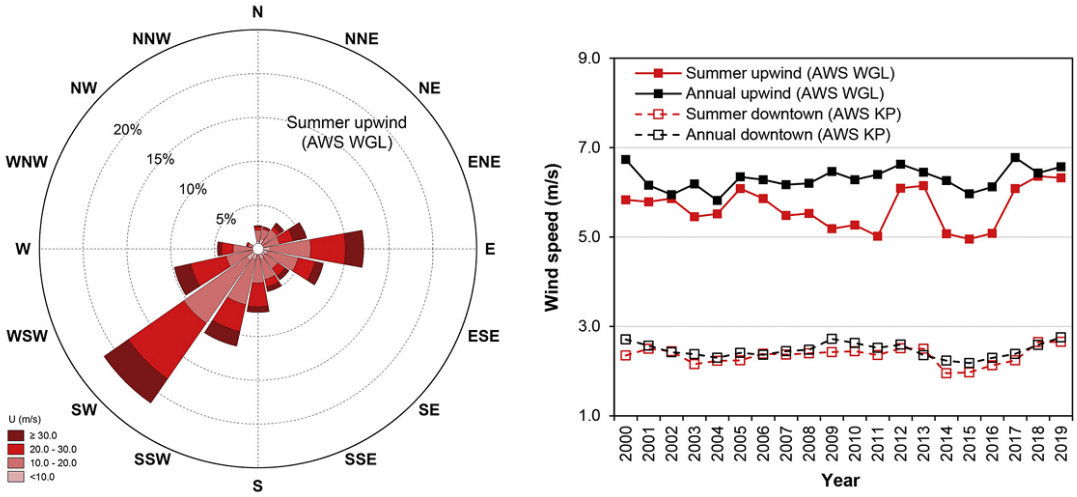

Fig. 2. Locations of the three LiDAR units (LiDAR CDA, LiDAR HKU, and LiDAR UST), Waglan Island automatic weather station (AWS WGL), as well as King's Park automatic weather station (AWS KP), and upper-air sounding system (AUSS KP).

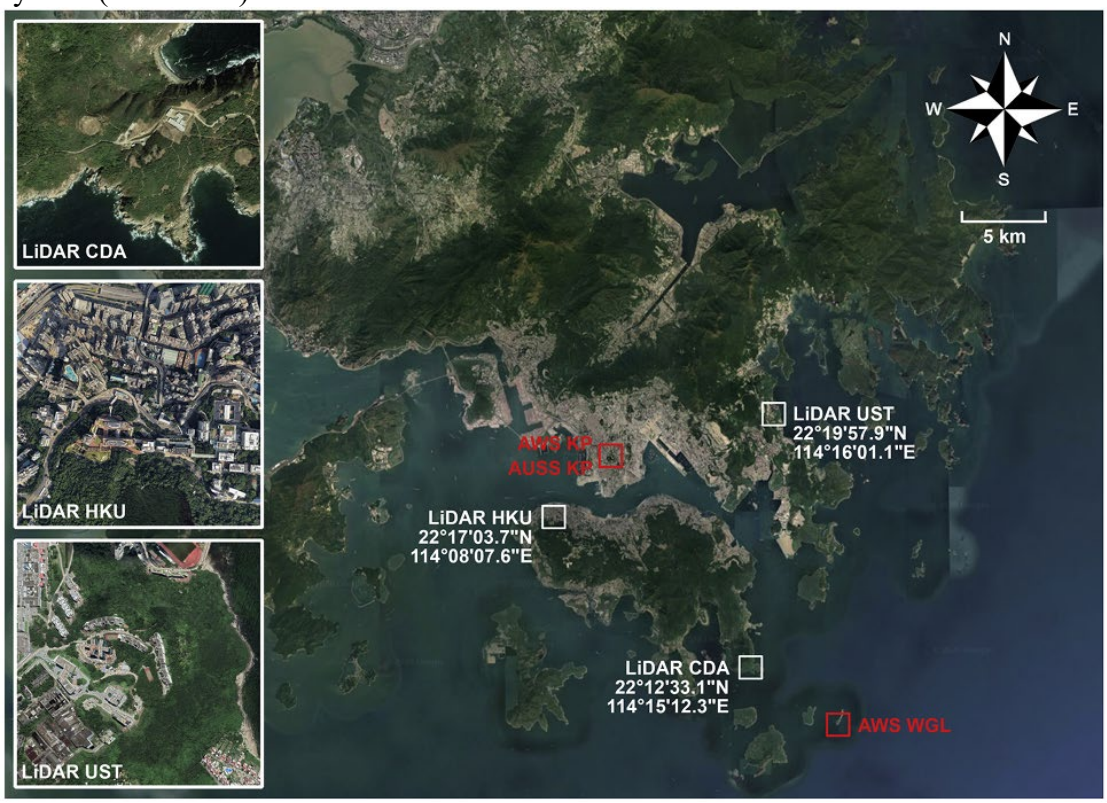

Fig. 3. Experimental design of the relative locations of the three LiDAR units: LiDAR CDA, LiDAR HKU, and LiDAR UST are designed for collecting the upwind, downtown, and downwind wind profiles under a prevailing southwest wind direction in Hong Kong (Remarks: The wind profiles and topography here serve only as a pictorial representation).

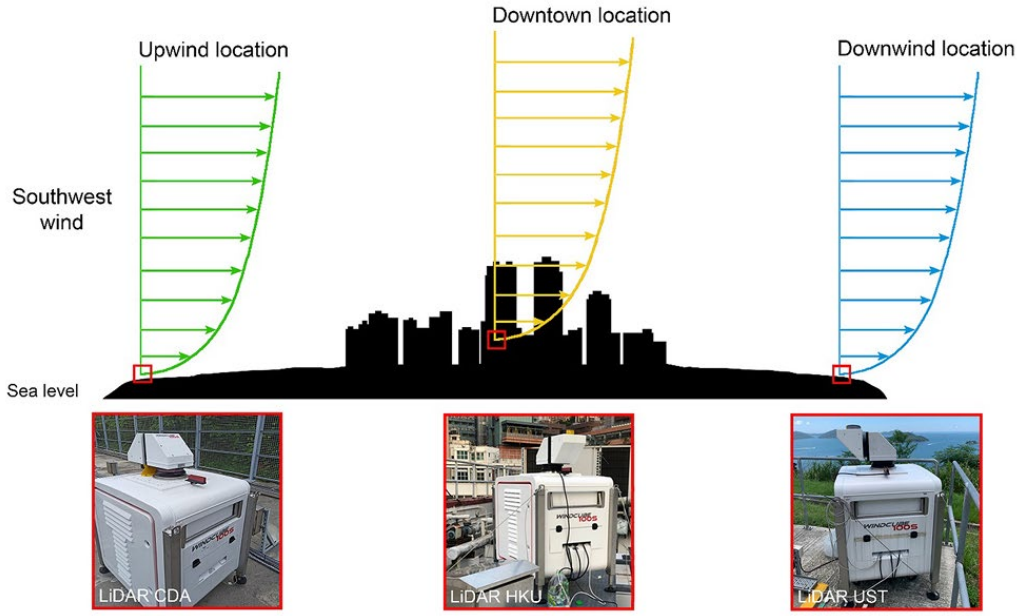

Fig. 4.Diagram of DBS scan mode: a) four azimuths, east, south, west and north, for emitting laser pulses; and b) an example of converting the detected radial wind speed along the east-tilted (VRE) and west-tilted (VRW) directions into the east-west horizontal component of wind speed (u).

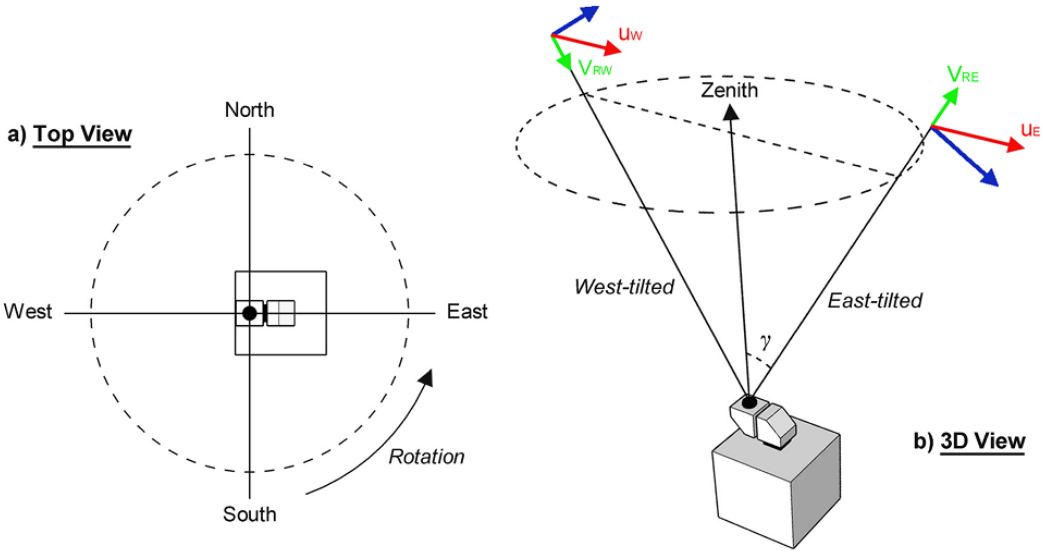

Fig. 5. Variations of daily average cloud coverage and total rainfall recorded at the HKO headquarters within the study period from June to August 2020.

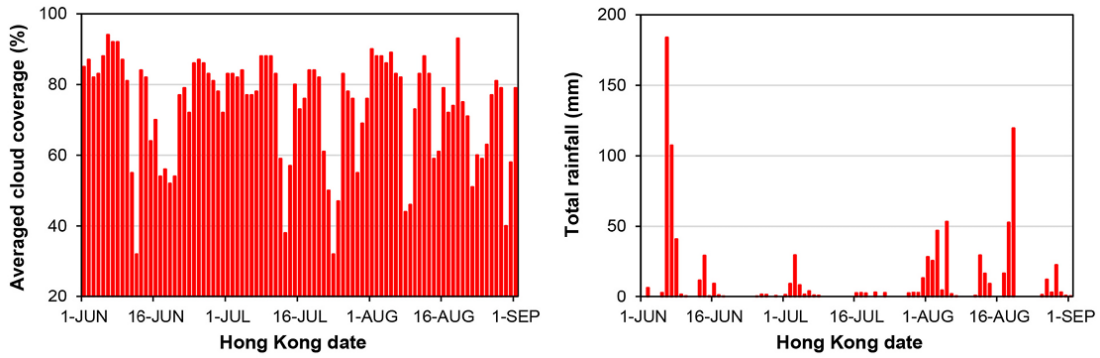

Fig. 6. Comparison of the hourly mean wind speed (m/s) and wind direction (degree) near the ground between LiDAR CDA and AWS WGL during the last week of June 2020.

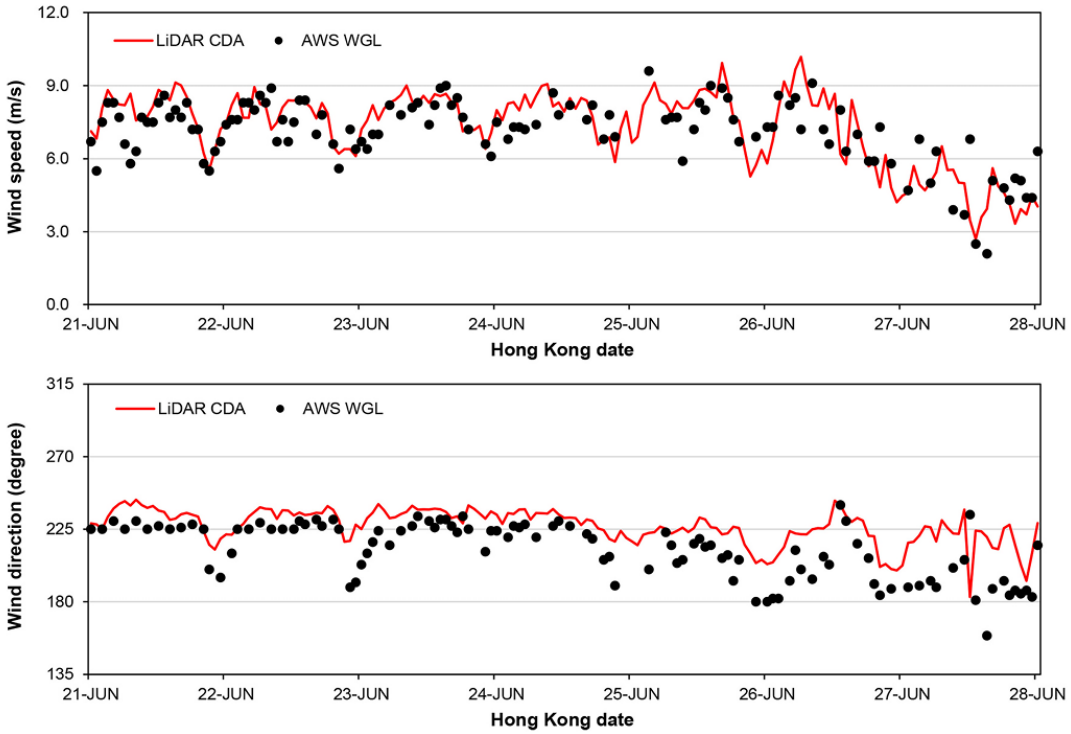

Fig.7. Comparisons of wind speed (U) profiles between LiDAR HKU and AUSS KP during the last week of June 2020 (LiDAR HKU: mean and standard deviation of the LiDAR data measured between 7.20 am/pm and 7.25 am/pm; and AUSS KP: single-time sounding data measured from 7.20 am to around 7.24 am).

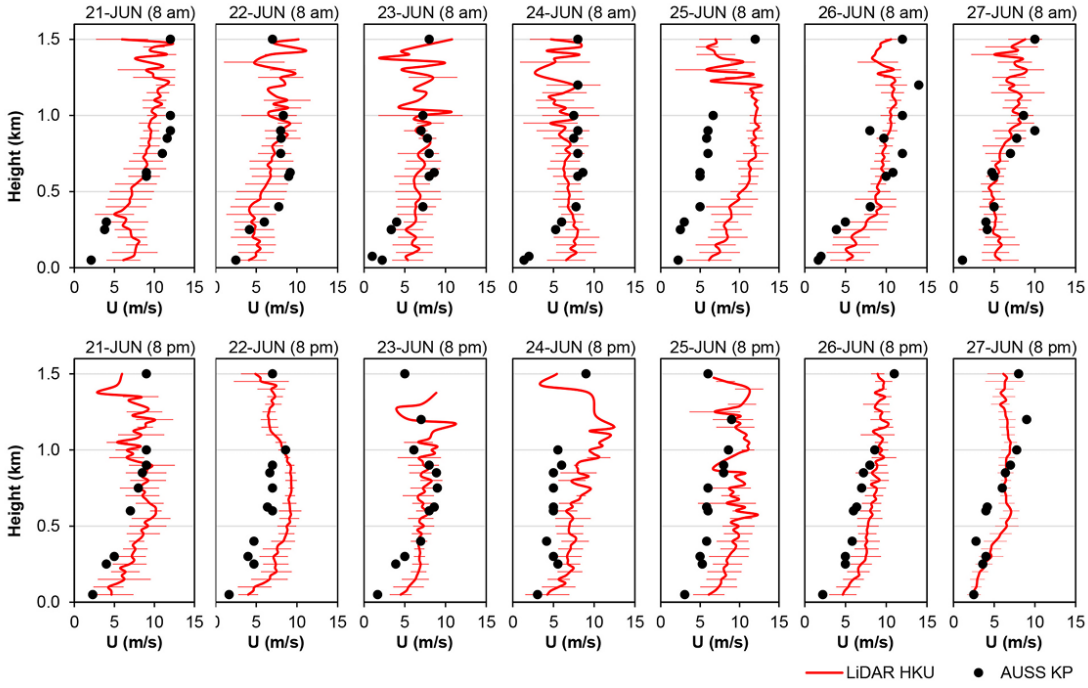

Fig. 8. Comparisons of wind direction profiles between LiDAR HKU and AUSS KP during the last week of June 2020 (LiDAR HKU: mean and standard deviation of the LiDAR data measured between 7.20 am/pm and 7.25 am/pm; and AUSS KP: single-time sounding data measured from 7.20 am to around 7.24 am).

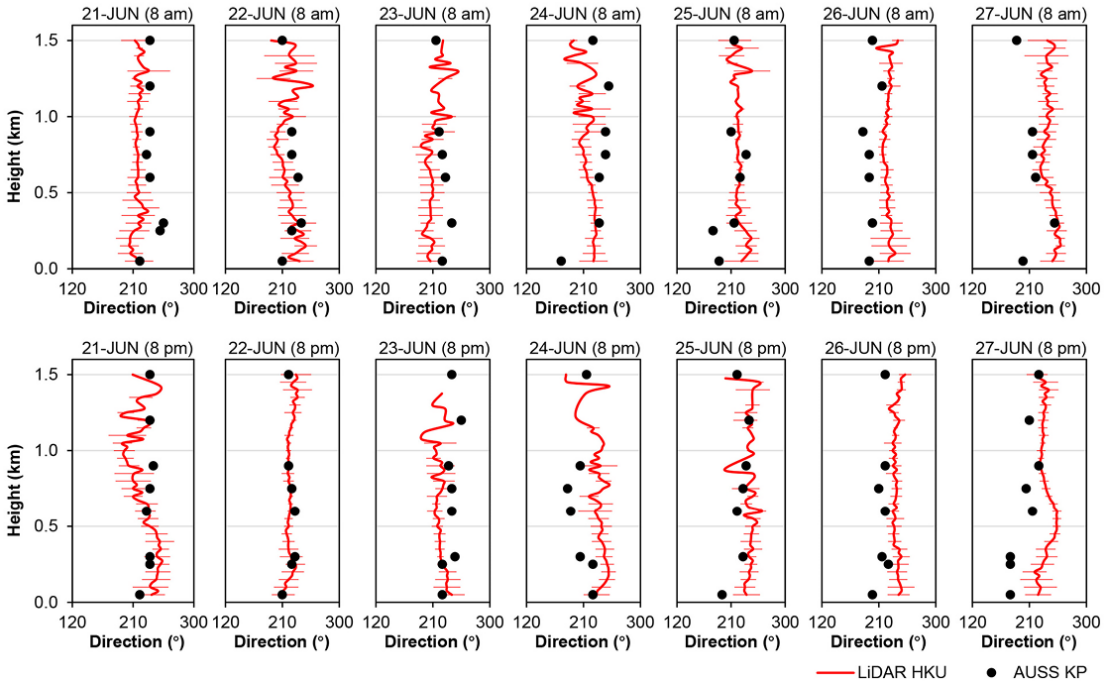

Fig. 9. The distribution of hourly mean wind speeds, and statistics of data availability, mean and standard deviation (S.D.) at AWS WGL and the three LiDAR locations during the study period from June to August 2020.

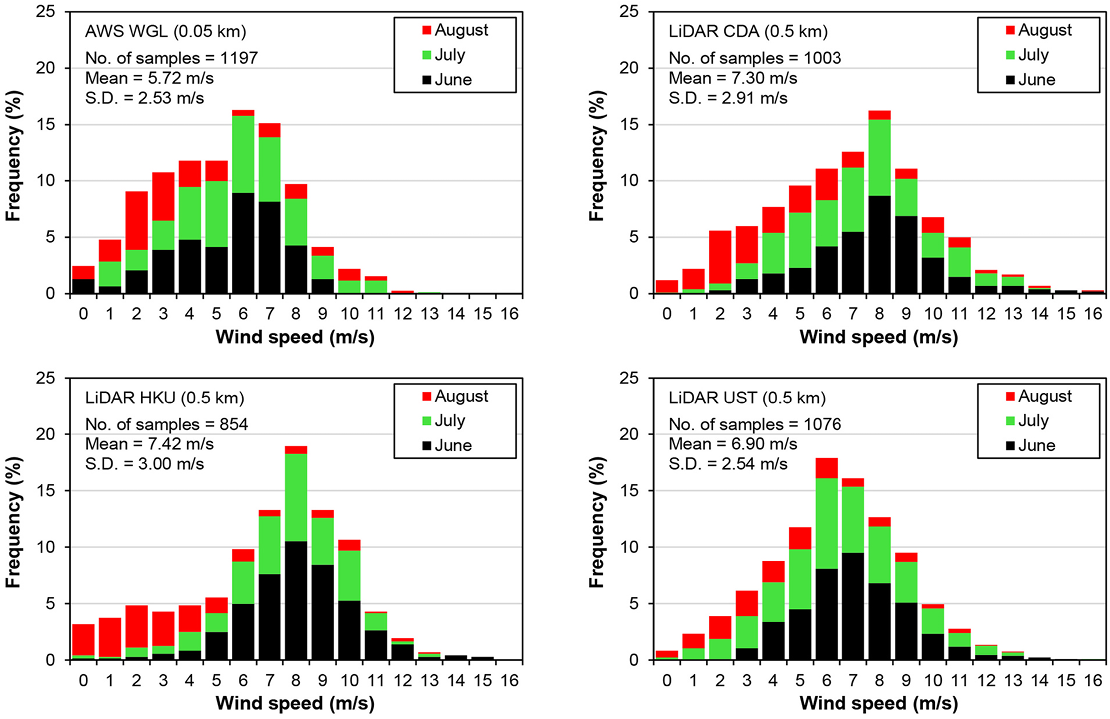

Fig. 10. Vertical hourly mean wind speed and wind shear profiles derived from LiDAR measurements at upwind, downtown, and downwind lo cations during the study period from June to August 2020.

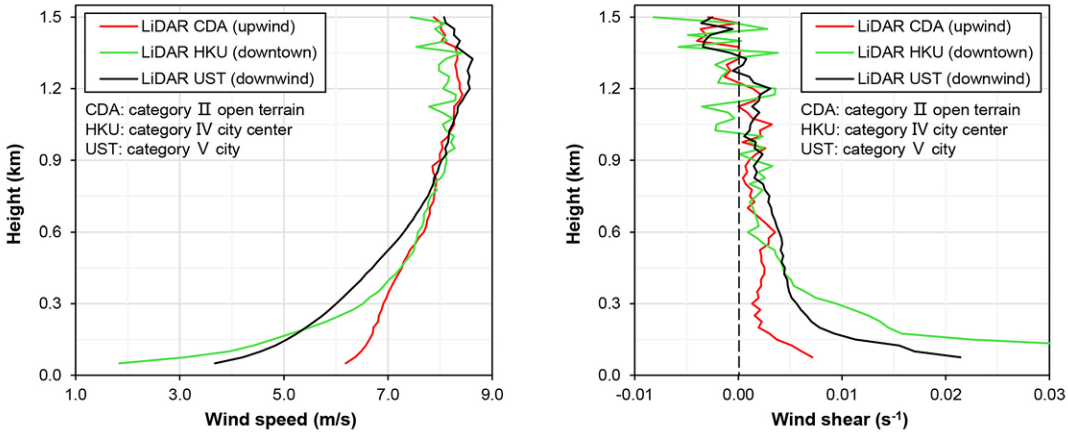

Fig. 11. Hourly mean and standard deviation of LiDAR wind speed profiles versus the mean wind speed profiles, as estimated by power-law equation (Eq. (1)), together with various exponents of terrain roughness (α) at upwind, downtown, and downwind locations.

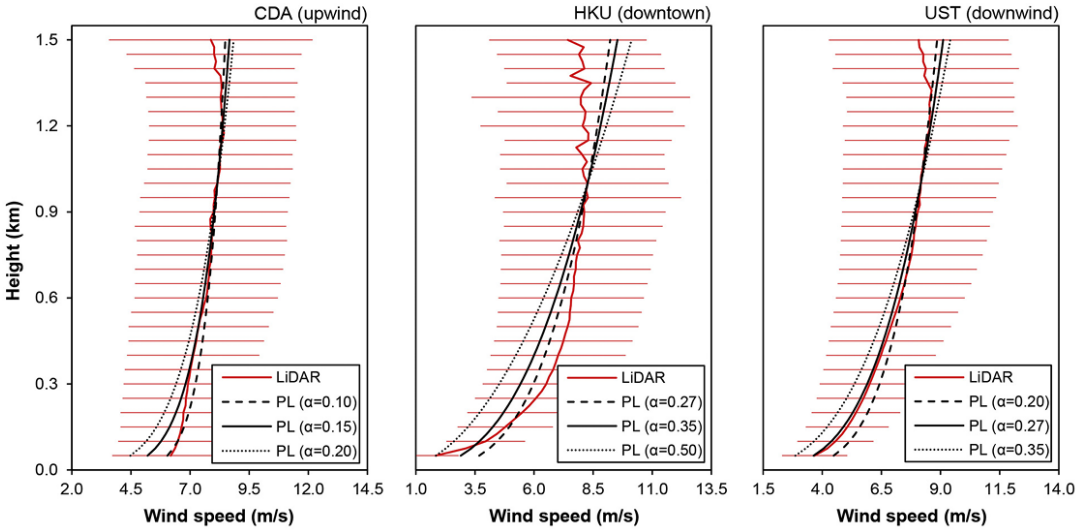

Fig. 12. Comparisons of LiDAR hourly mean wind speed profiles measured at daytime and nighttime.

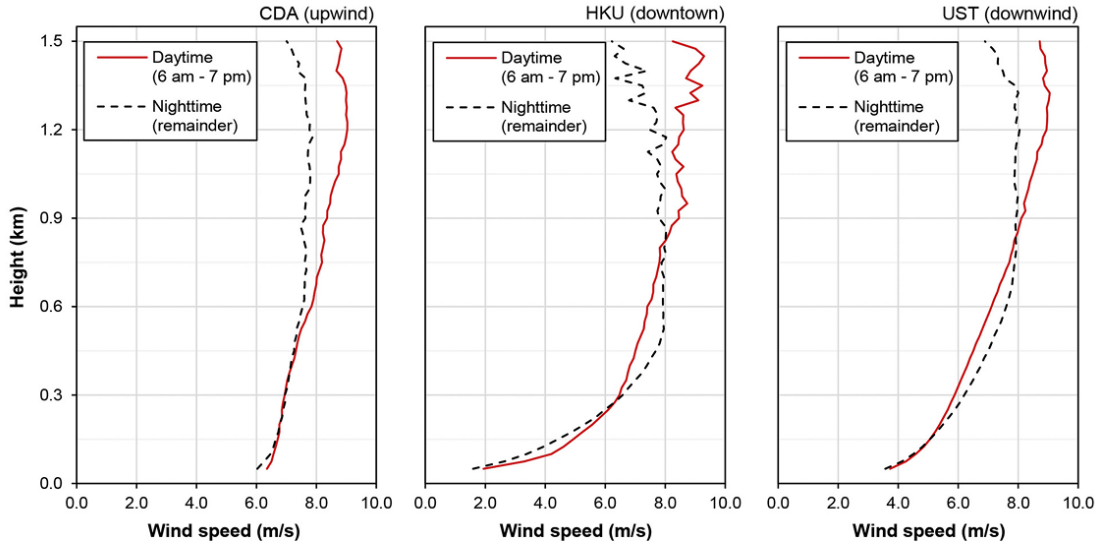

Fig. 13. Diurnal variations of hourly mean wind speed at various vertical levels during the study period from June to August 2020.

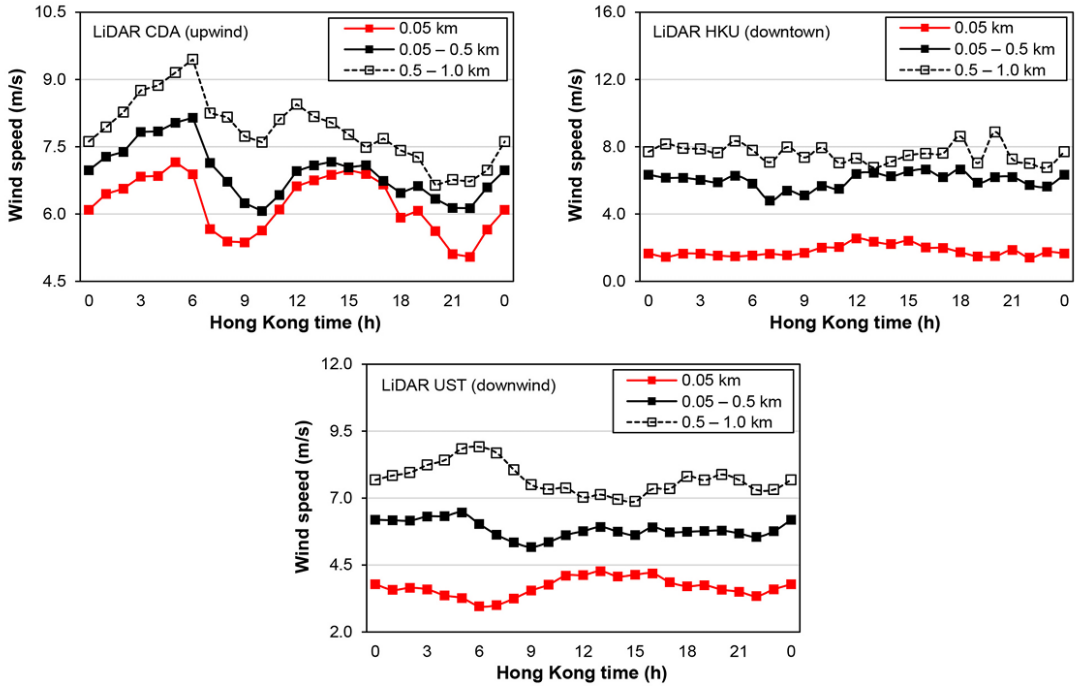

Fig. 14. Normalized mean wind velocity ratio profiles measured by the three LiDAR units, as well as the corresponding figures as estimated by boundary layer wind tunnel (BLWT), and meso-scale simulations of RAMS and WRF.

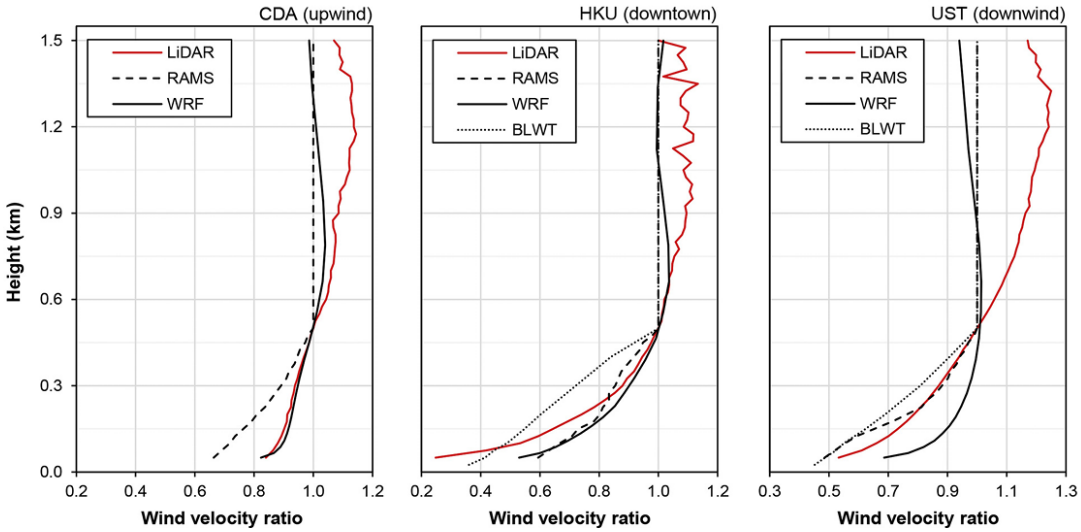

Table 1. Power-law exponents for estimation of terrain roughness (α) in various land-use categories (AIJ, 2015).

Category	α	Conditions of the construction site
I	0.10	Open, no significant obstruction, sea
II	0.15	Open, few obstructions, grassland, rice fields
III	0.20	Suburban, wooded terrain, few tall buildings (4–9 stories)
IV	0.27	City, tall buildings (4–9 stories)
V	0.35	City center, heavy concentration of tall buildings (higher than 10stories)

Table 2 .Comparison of various methods of obtaining vertical wind profiles in Hong Kong.

Data type	Pros	Cons
HKO's upper-air sounding data	• Real-site measurement • Long vertical data range (up to 30 km) • High vertical data resolution (around 11 m) • Moderate blind distance of near-ground data (0 to around 11 m)	• Low movability and single horizontal data point • Very low launching frequency of balloon (twice daily) • Vulnerable to adverse weather condition • Vulnerable to balloon drift
Wind tunnel data	• Multiple horizontal data points (13 sites) • Moderate near-ground blind distance of data (0 to 25 m)	• No real-site measurement • Short vertical data range (up to 0.5 km in full-scale) • Neutral stratification
Meso-scale simulated data (RAMS)	• Multiple horizontal data points (0.5 km × 0.5 km in whole territory) • Moderate blind distance of near-ground data (0 to 12.5 m)	• No real-site measurement • No real-time prediction and forecasting • Short vertical data range (up to 0.5 km) • Simplified physical and morphological features
Meso-scale simulated data (WRF)	• Real-time prediction and forecasting • Multiple horizontal data points (1 km × 1 km in whole territory) • Long vertical data range (up to 2.7 km)	• No real-site measurement • Simplified physical and morphological features
LiDAR wind data	• Real-site measurement • Long vertical data range (up to 3 km in DBS mode) • Moderate sampling rate (20 s in DBS mode) • High vertical data resolution (25 m) • High movability	• Long blind distance of near-ground data (0 to 50 m) • Vulnerable to adverse weather conditions (e.g., cloud, rainfall and fog)

Table 3. Statistics of wind conditions during the study period.

Wind condition	Number of hours (h)	Percentage
Southwest wind	1197	54.3%
Non-southwest wind	586	26.5%
Typhoons	104	4.7%
Missing data	321	14.5%
Total	2208	100.0%

Table 4. Power-law exponents of terrain roughness (α) in Hong Kong, validated by LiDAR observations in the summer.

Category	α	Conditions of the construction site
I	0.10–0.15	Upwind, undeveloped area
II	0.27	Downwind, suburban to rural area
III	0.35–0.5	Downtown, urban area